CHEMISTRY
A EUROPEAN JOURNAL

DOI: 10.1002/chem.200701705

Flutelike Porous Hematite Nanorods and Branched Nanostructures: Synthesis, Characterisation and Application for Gas-Sensing

Xinglong Gou,[a] Guoxiu Wang,*[a] Xiangyang Kong,[b] David Wexler,[a] Joseph Horvat,[a] Juan Yang,[a] and Jinsoo Park[a]

Abstract: Flute-like porous α-Fe_2O_3 nanorods and branched nanostructures such as pentapods and hexapods were prepared through dehydration and recrystallisation of hydrothermally synthesised β-FeOOH precursor. Transmission electron microscopy (TEM), high-resolution TEM and selected area electron diffraction analyses reveal that the nanorods, which grow along the [110] direction, have nearly hollow cavities and porous walls with a pore size of 20–50 nm. The hexapods have six symmetric arms with a diameter of 60–80 nm and length of 400–900 nm. The growth direction of the arms in the hexapod-like nanostructure is also along the [110] direction, and there is a dihedral angle of 69.5° between adjacent arms. These unique iron oxide nanostructures offer the first opportunity to investigate their magnetic and gas sensing properties. The nanostructures exhibited unusual magnetic behaviour, with two different Morin temperatures under field-cooled and zero-field-cooled conditions, owing to their shape anisotropy and magnetocrystalline anisotropy. Furthermore, the α-Fe_2O_3 nanostructures show much better sensing performance towards ethanol than that of the previously reported polycrystalline nanotubes. In addition, the α-Fe_2O_3 nanostructure based sensor can selectively detect formaldehyde and acetic acid among other toxic, corrosive and irritant vapours at a low working temperature with rapid response, high sensitivity and good stability.

Keywords: branched nanostructures · hematite · magnetic properties · porous materials · sensors

Introduction

Branched inorganic nanostructures, including tripods, tetrapods and other multipods, have recently attracted much attention, owing to their unique anisotropic crystal growth, novel properties and potential applications.[1,2] To date, multipod-like nanostructures have been observed in many inorganic materials with different crystallographic structures. For examples, a group of II–VI semiconductors having both the zinc blende and wurtzite structures, such as CdS, CdSe, CdTe, MnS, ZnS and ZnO, can form multipod-like nanostructures under the proper conditions,[3,4] owing to the different anisotropic growth rates of the zinc blende and wurtzite structures during the nucleation and growth processes. It has been determined that the branched multipods are initially nucleated in the zinc blende structure, and then grow anisotropically into multi-tips with wurtzite structures.[3] Moreover, some other groups found that the noble metals[5] and rock salt-phase PbS, PbSe and MnO[6] with highly symmetric crystal structures could also be grown as multipods. In this case, capping agents, such as cetyltriethylammonium bromide (CTAB) or poly(vinyl pyrrolidone) (PVP), were employed in the solution synthesis, which were selectively absorbed on different nucleated crystal surfaces, for controlling their crystal surface growth rates and producing the branched morphologies.[5,6] However, it still remains a challenge to fabricate other branched inorganic materials such as ferromagnetic or ferroelectric oxides with unique functionalities.

Hematite (α-Fe_2O_3) is the most stable iron oxide under ambient conditions with non-toxicity, low cost, high resistance to corrosion and environment-friendly features. It has been intensively investigated owing to its promising applications in gas sensors, rechargeable lithium-ion batteries, cata-

[a] Dr. X. Gou, Prof. Dr. G. Wang, Dr. D. Wexler, Dr. J. Horvat, Dr. J. Yang, Dr. J. Park
School of Mechanical, Materials and Mechatronic Engineering and Institute for Superconducting and Electronic Materials
University of Wollongong, Wollongong, NSW 2522 (Australia)
Fax: (+61) 2-4221-3112
E-mail: gwang@uow.edu.au

[b] Prof. Dr. X. Kong
School of Materials Science and Engineering
Shanghai Jiao Tong University, Shanghai 200030 (P.R. China)

Supporting information for this article is available on the WWW under http://www.chemeurj.org/ or from the author.

lysts, magnetic devices, photo-anodes for efficient water splitting by sunlight, waste-water treatment, pigments, biological and medical fields.[7–10] Various α-Fe_2O_3 micro- and nanostructures, such as dendritic micro-pines, 3D flowerlike architectures, urchin-like superstructures, nanospheres, nanorods, nanowires, nanotubes, nanobelts and nanorings, have been reported.[11–14] However, to the best of our knowledge, there has no report on the synthesis of porous α-Fe_2O_3 branched nanostructures so far.

In this paper, we report the synthesis of α-Fe_2O_3 bamboo flute-like porous nanorods and hexapod-like nanostructures through a surfactant-free hydrothermal process with subsequent calcination of the hydrothermally obtained precursors. The microstructures of the flutelike porous nanorods and hexapods were analysed by transmission electron microscopy (TEM), high-resolution TEM (HRTEM) and selected area electron diffraction (SAED). We found that the arms of a hexpodlike nanostructure and an individual nanorod have the same growth direction of [110]. Furthermore, the unique porous and multipod-like nanostructures of the as-prepared α-Fe_2O_3 were expected to endow them with enhanced performance. We measured the magnetism and gas-sensing performance of the as-prepared α-Fe_2O_3 nanostructures. Magnetic measurements revealed weak ferromagnetic behaviour at room temperature, with much lower Morin transition temperatures than for bulk materials. We found that the field-cooled (FC) and zero-field-cooled (ZFC) magnetisations of the as-synthesised α-Fe_2O_3 nanostructures under an applied field of 500 Oe exhibited two different Morin temperatures. Moreover, the as-synthesised α-Fe_2O_3 nanostructures show excellent sensing performance towards some flammable, toxic and corrosive gases.

Results and Discussion

Structure and morphology characterisation: The α-Fe_2O_3 porous nanorods and branched nanostructures were synthesised by dehydration and recrystallisation of β-FeOOH precursor, which was obtained from the hydrothermal reaction of $FeCl_3$ with urea in an aqueous solution, as described in Equations (1)–(3). Figure 1 shows the X-ray diffraction (XRD) patterns of the precursor and the final product. All the diffraction peaks of the hydrothermally obtained precursor (pattern a) can be indexed to tetragonal β-FeOOH (JCPDS Card No. 34–1266). After being heated in air at 500 °C for 5 h, the precursor was completely converted to pure rhombohedral phase α-Fe_2O_3 (pattern b, JCPDS Card No. 33–0664). Equation (3) explains that the conversion of β-FeOOH to α-Fe_2O_3 is a solid-state reaction, and only pure Fe_2O_3 is left as the final product, because the H_2O produced is expelled as vapour. So this strategy is a relatively environmentally friendly chemical synthetic route for large-scale preparation of α-Fe_2O_3 nanostructures.

$$NH_2CONH_2 + 3\,H_2O \rightarrow 2\,NH_3 \cdot H_2O + CO_2 \quad (1)$$

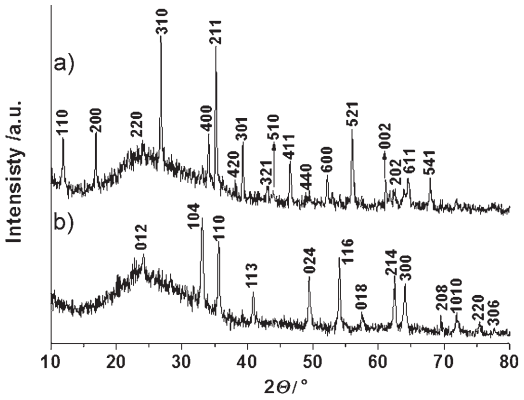

Figure 1. XRD patterns of the a) as-prepared β-FeOOH precursor and b) the α-Fe_2O_3 nanostructures.

$$FeCl_3 + 3\,NH_3 \cdot H_2O \rightarrow FeOOH + 3\,NH_4Cl + H_2O \quad (2)$$

$$2\,FeOOH \rightarrow Fe_2O_3 + H_2O \quad (3)$$

The morphology of the as-prepared nanostructures was characterised by TEM and HRTEM. Figure 2a shows a low magnification TEM image of the final product. The inset contains the electron diffraction (ED) pattern, which was taken from the whole area. The diffraction ring indicates the polycrystalline nature of α-Fe_2O_3 and is highly consistent with the XRD results. It is obvious that the as-prepared α-Fe_2O_3 was composed of porous nanorods and multipod-like nanostructures, such as those marked with frames. The nanorods have diameters of 60–80 nm and lengths of 400–900 nm; whereas the branched nanostructures have five or six arms symmetrically distributed. Under higher magnification (Figure 2b) we can see that the porous nanorods tend to organise themselves in a parallel alignment, owing to weak van der Waals attraction. In Figure 2c an individual nanorod has been further magnified to show its flutelike structure, its nearly hollow cavity and porous wall. The size of the pores in the wall is in the range of 20–50 nm, which was confirmed by Brunauer–Emmett–Teller (BET) surface area measurement and the pore size distribution analysis (See Figure S1 in the Supporting Information). This porous network is believed to favour for gas sensing. The clear spots in the SAED pattern (the inset in Figure 2c) reveal the single crystalline nature of the individual α-Fe_2O_3 nanorod, with a growth direction of [−110]. Apart from the porous nanorods, some branched nanostructures were also observed. Figures 2d and 2e show typical hexapod and pentapod nanostructures, respectively. The six arms of a hexapod are distributed octahedrally with a fourfold axis of symmetry, whereas the five arms of a pentapod are aligned like a tetragonal pyramid. The diameters and lengths of the arms in both kinds of branched nanostructures are equivalent to those of individual nanorods.

The formation of the branched multipod-like nanostructure for hematite α-Fe_2O_3 is of considerable interest. Figure 3a shows the TEM image of a tilted hexapod. It was found that the branched structure is also porous, owing to

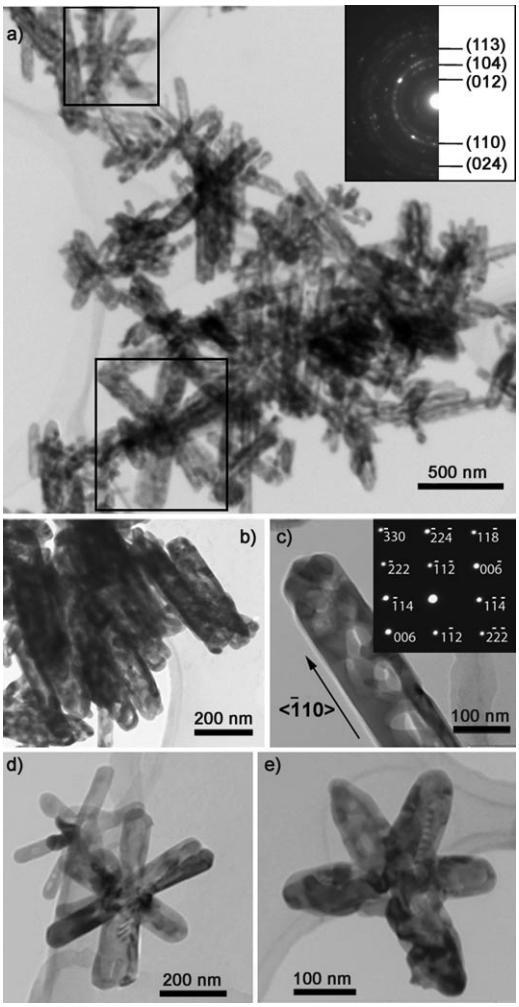

Figure 2. The morphology of the as-synthesised α-Fe_2O_3 nanostructures. TEM images: a) An overall view (inset is the ED pattern taken from the whole area), and the frame indicates typical multipod-like structures, b) aligned porous nanorod bundles, c) a single flutelike porous nanorod (inset is the corresponding SAED pattern), d) hexapod nanostructures, and e) a pentapod nanostructure.

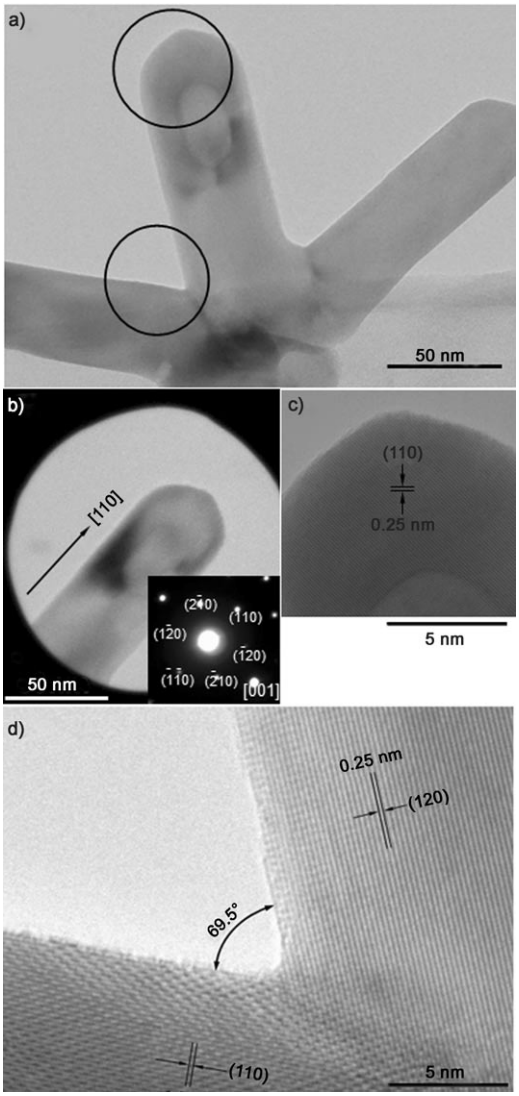

Figure 3. Microstructure of the hexapod nanostructure. TEM images: a) of a tilted α-Fe_2O_3 hexapod nanostructure and b) tip of the arm circled in a), with the inset showing the corresponding SAED pattern. HRTEM images; c) higher resolution image of b) and d) image of the second circled area in a) showing the joint of two arms with a dihedral angle of 69.5 °C.

dehydration of the precursor during the heating process. The tip of one arm (marked with a circle in Figure 3a) was brought into focus, as is shown in Figure 3b, along with the corresponding SAED pattern, to indicate its single crystalline nature with a growth direction of [110], which is the same as that of the straight nanorod. The corresponding HRTEM image (Figure 3c) shows regular lattice fringes with a spacing of 0.25 nm, which is highly consistent with the *d* value of the (110) plane. The point where two arms join (marked with a circle in Figure 3a) was further analysed by HRTEM (Figure 3d). The distinct lattice fringes in both arms and the core of the joint reveal unambiguously that the hexapod nanostructure is a single crystal in essence and that the growth directions of both arms are in the [110] direction. There is a dihedral angle of 69.5° between the two arms.

The addition of urea and the hydrothermal treatment played an important role in obtaining the α-Fe_2O_3 branched nanostructures. If $FeCl_3$ is hythrothermally treated without addition of urea, irregular aggregates are obtained. If the solution of $FeCl_3$ and urea is refluxed at 120 °C for 10 h, the product is composed of needle-like particles and irregular aggregates (not shown here), which indicates that the addition of urea could promote, to a certain extent, the growth of one dimensional shapes. Here, urea may have a similar role to that of some of the inorganic salts in the preparation of 1D nanomaterials.[12a,b] Compared to other inorganic salts, the hydrolysis products of urea are CO_2 and NH_3, as indicated in Equation (1), and thus do not introduce any impurities into the target materials. So we combined the advantages of the hydrothermal technique with the slow release of ammo-

nia by the decomposition of urea to control the hydrolysis of Fe^{3+} and the crystallisation of the resulting β-FeOOH precursor, and finally synthesised the branched α-Fe_2O_3 nanostructures though calcination of the iron oxyhydroxide precursor.

Magnetic behaviour: The magnetic properties of hematite in the bulk form and on the nanoscale have been intensively investigated, owing to their diverse applications in magnetic storage devices, spin electronics devices, drug delivery, tissue repair engineering and magnetic resonance imaging.[15,8b] Bulk α-Fe_2O_3, besides the Néel temperature ($T_N = 955$ K), has a first-order magnetic transition at $T = 263$ K, which is called the Morin transition, and the corresponding temperature is termed the Morin transition temperature (T_M). Below T_M, the antiferromagnetically (AF) ordered spins are oriented along the *c*-axis. Above T_M, the AF spins lie in the basal plane of the crystal with a slight canting away from the plane. This canting results in a weak ferromagnetism.[15] However, the α-Fe_2O_3 nanoparticles can exhibit antiferromagnetic, ferromagnetic and superparamagnetic behaviour, depending strongly on the size, shape, porosity and the preparation conditions of the materials.[15,8b] Owing to the unique porous and branched nanostructures of the prepared α-Fe_2O_3 samples (Figures 2 and 3), it is worthwhile to investigate its magnetic behaviour. The temperature dependence of magnetic moments for the as-synthesised α-Fe_2O_3 nanostructures under zero-field-cooled (ZFC) and field-cooled (FC) conditions from $T = 20$ to 300 K are shown in Figure 4a. A field of 500 Oe was applied and the sample was cooled or warmed with a sweep rate of temperature across the transition of 0.2 K min^{-1}. A sharp decrease in magnetisation was observed at $T = 252$ °C for ZFC conditions, displaying the characteristic behaviour for α-Fe_2O_3. In contrast to the bulk counterpart, the Morin temperature for the FCC and ZFC conditions differed notably in the temperature range studied. Although T_M is reported to depend on the specific shape, size and porosity of the nanoparticles,[12a] its value has always been the same for FCC and ZFC measurements. It is interesting that the ZFC and FCC branches of our samples have different Morin temperatures, which were determined by the sharp peaks in the corresponding differential curves as $T = 245$ K and 233 K respectively (inset in Figure 4a). We suggest that surface spins in the nanorods and branched nanostructures re-orient themselves upon thermal (field) cycling, inducing a different interaction ratio for in-plane and out-plane interactions, owing to their shape anisotropy and magnetocrystalline anisotropy. To better understand the effects of the shapes on the magnetism of α-Fe_2O_3 nanostructures, further investigations should be performed.

The field dependence of the magnetisation at $T = 273$ K (Figure 4b) confirms the weak ferromagnetism above T_M. The coercive force at $T = 273$ K of 0.71 T is larger than that of spherical hematite. This might be a result of both the shape anisotropy and the magnetocrystalline anisotropy of the porous and branched α-Fe_2O_3 nanostructures, which

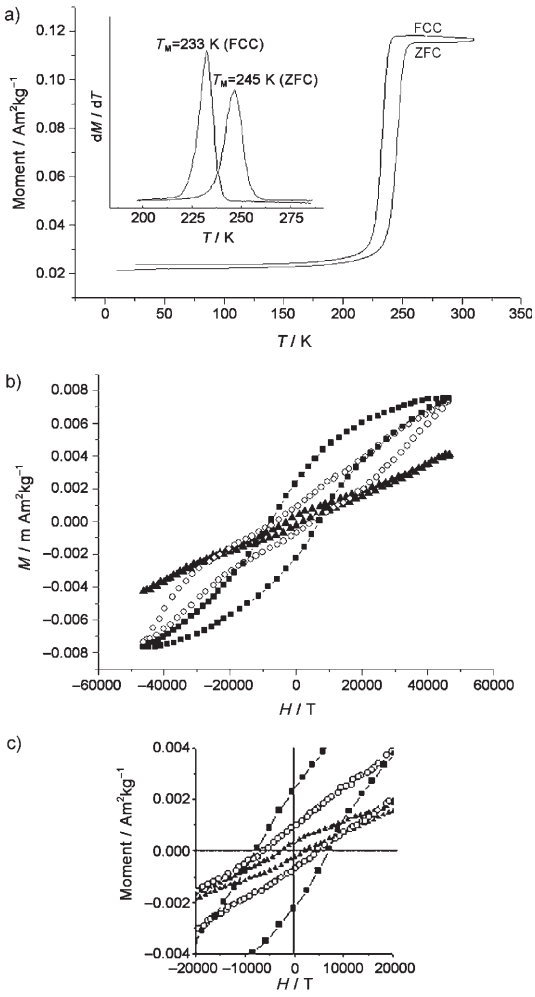

Figure 4. Magnetic behaviour of the as-prepared α-Fe_2O_3 nanostructures: a) Temperature dependences of ZFC and FCC magnetisation for an applied field of 500 Oe. The inset shows the corresponding differential ZFC and FCC curves. b) Magnetic hysteresis loops at $T = 273$(■), 210(○) and 10 K (△). c) A magnified view of b).

exert an influence on their magnetic properties. Furthermore, at lower temperatures, for example at $T = 210$ K and 10 K, these materials still show hysteresis loops that are indicative of the presence of ferromagnetic components (Figure 4c).

Gas-sensing performance: The increasing concern over environmental monitoring and safety demands in industry have generated great interest in the development and optimisation of semiconducting gas sensors with respect to their sensitivity, response rate, gas selectivity and economic efficiency (low manufacturing costs, low operating temperatures).[16,17] Polycrystalline Fe_2O_3 nanotubes have been reported as having good ethanol gas sensing performance.[7a] Stimulated by the similarities of porous structure and high specific surface area between the polycrystalline nanotubes and the as-prepared porous α-Fe_2O_3 nanorods and branched nanostructures, we investigated the sensing performance of the as-prepared nanostructures towards a variety of flammable, toxic

and corrosive gases such as ethanol, acetone, gasoline, heptane, formaldehyde, toluene, acetic acid and ammonia.

Figure 5a shows a schematic diagram of the sensor system. The gas sensor was fabricated by depositing the as-synthesised α-Fe_2O_3 nanostructures as a thin film on a ceramic tube with previously printed Au electrodes and Pt conducting wires. The working temperature of the sensor can be controlled by adjusting the heating voltage ($V_{heating}$) across a resistor inside the ceramic tube. A reference resistor is put in series with the sensor to form a complete measurement circuit. In the test process, a working voltage ($V_{working}$) was applied. By monitoring the voltage (V_{output}) across the reference resistor, the response of the sensor in air or in a test gas can be measured. The response characteristics towards ethanol of the sensors based on the as-synthesised α-Fe_2O_3 nanostructures and on commercial powder (the XRD pattern and SEM image of which was respectively shown in Figures S2 and S3 in the Supporting Information) at a working temperature of 150 °C and 30 % relative humidity (RH) is displayed in Figure 5b. It can be seen that V_{output} values increased abruptly on the injection of ethanol and then decreased rapidly and recovered to their initial value after the test gas was released. From Ohm's law, the electric resistance of the sensor accordingly underwent a decreasing and increasing process when the test gas was turned on and off, respectively, which is quite consistent with the sensing behaviour of *n*-type semiconductor sensors.[16] The response magnitude of the sensor based on the as-synthesised α-Fe_2O_3 nanostructures improved dramatically with increasing concentration of the test gas and was always higher than that of the commercial powder. This means that the Fe_2O_3 nanostructures are more sensitive to ethanol than the commercial powder. After many cycles between the test gas and fresh air, the voltage of the reference resistor and the resistance of the sensor could recover their initial states, which indicates that the sensor has good reversibility. The response time and recovery time (defined as the time required to reach 90 % of the final equilibrium value) of the nanostructure-based sensors were only 1–3 and 4–8 s, respectively. The response characteristic curves of the sensors for other gases are similar to that for ethanol and are not shown here.

The gas sensitivity is defined as the ratio of the stationary electrical resistance of the sensor in the test gas (R_{gas}) and in air (R_{air}), i.e., $S = R_{gas}/R_{air}$. The sensitivity of the sensors

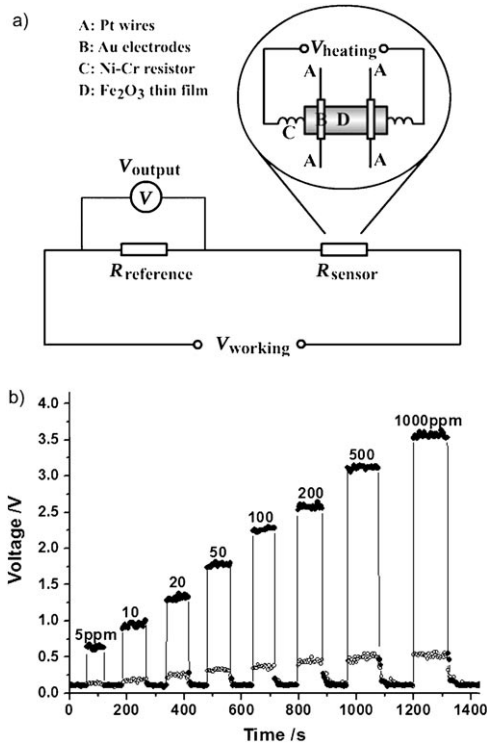

Figure 5. a) Schematic illustration of the gas sensor measurement system. b) Real-time ethanol sensing characteristics of sensors based on the prepared α-Fe_2O_3 nanostructures (?kv) and on commercial Fe_2O_3 powder (?kl).

based on the nanostructures and on the commercial powder as a function of ethanol vapour concentration is shown in Figure 6a. It can be seen that the sensitivity of the α-Fe_2O_3

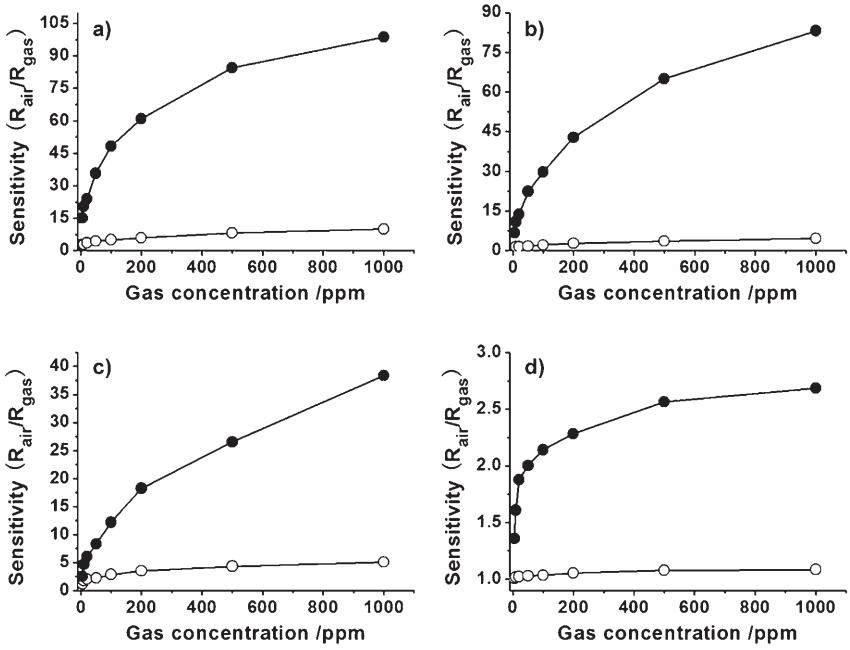

Figure 6. Sensitivity of the sensors based on the as-prepared α-Fe_2O_3 nanostructures (●) and on the commercial powder (○) as a function of the vapour concentration of some flammable gases; a) ethanol, b) acetone, c) 92# gasoline and d) heptane.

nanostructures is about five times higher than that of the commercial powder at 5 ppm of ethanol vapour. Furthermore, this discrepancy is much magnified with increasing ethanol vapour concentration, and reaches a tenfold extent at 1000 ppm. This result indicates that the sensing performance of the as-prepared α-Fe_2O_3 nanorods and branched nanostructures is better than that of the previously reported polycrystalline nanotubes,[7a] considering the lower preparation cost and higher sensitivity. The improvement of the sensing performance of the present α-Fe_2O_3 nanostructures may be attributed to three main aspects. In the first place, the grain size of the as-prepared nanorods and branched nanostructures is much smaller, leading to higher specific surface area, which was measured to be 125.2 $m^2 g^{-1}$. The BET surface area of commercial α-Fe_2O_3 powders is 18 $m^2 g^{-1}$. Secondly, the abundant pores distributed in three-dimensional space can facilitate the diffusion of the test gas and improve the kinetics of both the reaction of the test gas with surface-adsorbed oxygen and the replacement of the latter from the gas phase.[17] On the other hand, the contact electronic resistance of grains should be taken into consideration. The high interconnectivity of the prepared single crystalline nanostructures can enhance the transport of electrons and increase the electronic conductance.

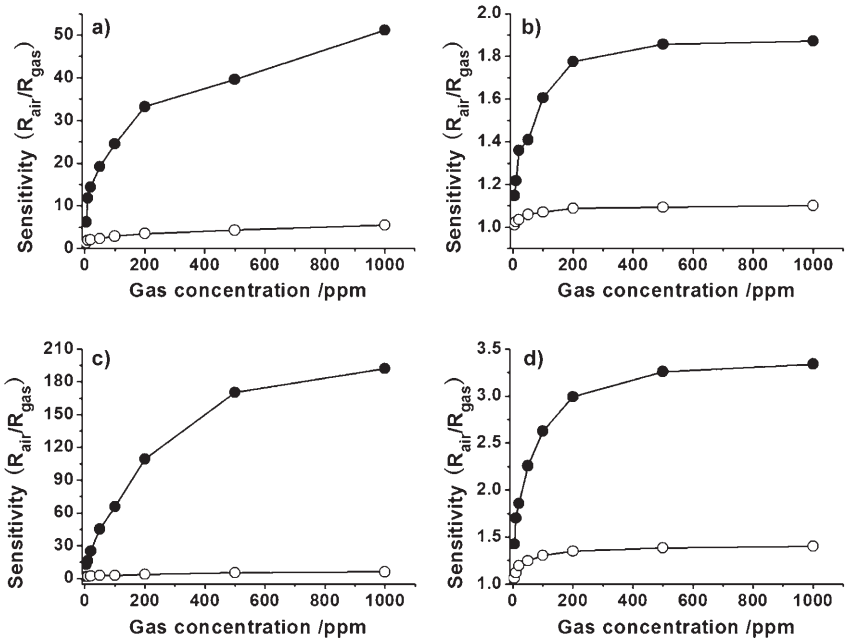

Figure 7. Sensitivity of the sensors based on as-prepared α-Fe_2O_3 nanostructures (●) and commercial powder (○) as a function of the vapour concentration of some toxic and corrosive gases; a) formaldehyde, b) toluene, c) acetic acid and d) ammonia.

Apart from ethanol, some other flammable and explosive gases such as acetone, 92# gasoline and heptane were also investigated, and the corresponding results are shown as Figure 6b–d, respectively. Obviously, the sensitivity of the as-synthesised α-Fe_2O_3 nanostructures was always much better than that of the commercial powder no mater what kind of gas was tested. The sensitivity of the nanostructure sensor decreased in the sequence of ethanol, acetone and gasoline. However, the sensor could barely detect heptane, even when its actual concentration was very high (for example 1000 ppm), indicating that the α-Fe_2O_3 nanostructure based sensor has a degree of selectivity to flammable and explosive gases.

Formaldehyde (HCHO) and toluene are well known toxic chemicals and hazardous to our health and environment. Acetic acid and ammonia are corrosive liquids and can give off strongly irritating gases. Therefore, efficient chemical sensors to detect these gases are demanded. Figure 7 shows the measurement results. In general, the sensing performance of the as-prepared nanostructures is much better than that of the commercial powder. In regard to the detection of toxic gases, the α-Fe_2O_3 nanostructures exhibited high sensitivity ($S=6$, Figure 7a) to HCHO vapour, even though its concentration was very low (5 ppm). In addition, with increasing HCHO concentration (5–200 ppm) the sensitivity increased exponentially, then linearly (200–1000 ppm), and reached 51 in the presence of 1000 ppm of HCHO vapour. However, the sensor is not sensitive to toluene (Figure 7b). As for the corrosive and irritant gasses, the sensor displays high sensitivity to acetic acid (Figure 7c), with S reaching as high as $S=192$ in the presence of 1000 ppm of acetic acid vapour. Here, the unusual high sensitivity of the sensor to acetic acid may be caused by the strong chemiadsorption of acetic acid on the surface of the Fe_2O_3, owing to the strong coordination of carboxyl to Fe^{3+}. In contrast, it was not sensitive to ammonia (Figure 7d). These results revealed that the as-prepared α-Fe_2O_3 nanostructures can selectively detect formaldehyde and acetic acid with high sensitivity.

It was found that the on and off responses could be repeated after continuous measurement for two weeks without observing any changes in the signal, illustrating the good reversibility and stability of the α-Fe_2O_3 nanostructure based sensor.

Conclusion

In summary, flute-like porous α-Fe_2O_3 nanorods and branched nanostructures, such as pentapods and hexapods, were synthesised by the dehydration and recrystallisation of

a hydrothermally produced β-FeOOH precursor. TEM, HRTEM and SAED analyses revealed that the hexapod nanostructures have six symmetric arms with a dihedral angle of 69.5°. The arms of a hexapod nanostructure grow along the [110] direction, which is the same direction as for an individual porous nanorod. The as-prepared α-Fe_2O_3 nanostructures exhibited unique magnetic properties, with two different Morin temperatures under FCC and ZFC conditions. The as-prepared α-Fe_2O_3 nanostructures show excellent sensing performances in selectively detecting ethanol, formaldehyde and acetic acid. These results highlight the potential application of the as-prepared α-Fe_2O_3 porous and branched nanostructures in monitoring flammable, toxic and corrosive gases.

Experimental Section

Synthesis: Flute-like porous α-Fe_2O_3 nanorods and branched nanostructures were prepared through a two-step process including hydrothermal synthesis of β-FeOOH precursor and calcination of the obtained precursor. First, a mixture of $FeCl_3$ (2 mmol) and urea (5 mmol) was hydrothermally treated at 120 °C for 10 h, a brown-yellow precipitate was collected, washed with distilled water and absolute ethanol, and finally dried under a vacuum at 60 °C for 4 h to obtain the precursor. Then, the precursor was heated in air at 500 °C for 5 h and converted completely to the α-Fe_2O_3 nanostructures.

Characterisation: The as-prepared samples were characterised by means of X-ray diffraction (XRD, $Cu_{K\alpha}$ radiation, Philips 1730), scanning electron microscopy (JEOL 6460), transmission electron microscopy (TEM) and high-resolution TEM (HRTEM, JEOL 2011). The BET surface area measurement was performed by using a Quanta Chrome Nova 1000 Gas Sorption Analyser. Magnetic properties were measured by using a Quantum Design MPMS XL SQUID magnetometer. Gas sensing measurements were carried out by means of a WS-30 A system.

Acknowledgements

This work was financially supported by the Australian Research Council (ARC) through an ARC Discovery Project - Synthesis of nanowires and their application as nanosensors for chemical and biological detection (DP0559891).

[1] a) D. J. Milliron, S. M. Hughes, Y. Cui, L. Manna, J. Li, L. Wang, A. P. Alivisatos, *Nature* **2004**, *430*,190–195; b) T. Mokari, E. Rothenberg, I. Popov, R. Costi, U. Banin, *Science* **2004**, *304*, 1787–1790.

[2] a) D. Wang, C. M. Lieber, *Nat. Mater.* **2003**, *2*, 355–356; b) S. C. Glotzer, M. J. Solmon, *Nat. Mater.* **2007**, *6*, 557–562.

[3] a) Y. Jun, S. Lee, N. Kang, J. Cheon, *J. Am. Chem. Soc.* **2001**, *123*, 5150–5151; b) L. Manna, E. C. Scher, A. P. Alivisatos, *J. Am. Chem. Soc.* **2000**, *122*, 12700–12706; c) L. Manna, E. J. Milliron, A. Meisel, E. C. Scher, A. P. Alivisatos, *Nat. Mater.* **2003**, *2*, 382–385.

[4] a) Y. Jun, Y. Jung, J. Cheon, *J. Am. Chem. Soc.* **2002**, *124*, 615–619; b) G. Z. Shen, Y. Bando, J. Q. Hu, D. Golberg, *Appl. Phys. Lett.* **2007**, *90*, 123101; c) Y. Qiu, S. Yang, *Adv. Funct. Mater.* **2007**, *17*, 1345–1352.

[5] a) N. Zettsu, J. M. McLellan, B. Wiley, Y. Yin, Z. Li, Y. Xia, *Angew. Chem.* **2006**, *118*, 1310–1314; *Angew. Chem. Int. Ed.* **2006**, *45*, 1288–1292; b) X. Teng, H. Yang, *Nano Lett.* **2005**, *5*, 885–891; c) S Chen, Z. L. Wang, J. Ballato, S. H. Foulger, D. L. Carroll, *J. Am. Chem. Soc.* **2003**, *125*, 16186–16187.

[6] a) Y. Zhang, L. Guo, P. Yin, R. Zhang, Q. Zhang, S. Yang, *Chem. Eur. J.* **2007**, *13*, 2903–2907; b) K. Cho, D. V. Talapin, W. Gaschler, C. B. Murray, *J. Am. Chem. Soc.* **2005**, *127*, 7140–7147; c) D. Zitoun, N. Pinna, N. Frolet, C. Belin, *J. Am. Chem. Soc.* **2005**, *127*, 15034–15035.

[7] a) J. Chen, L. Xu, W. Li, X. Gou, *Adv. Mater.* **2005**, *17*, 582–585; b) G. Jain, M. Balasubramanian, J. J. Xu, *Chem. Mater.* **2006**, *18*, 423–434.

[8] a) M. Hermanek, R. Zboril, I. Medrik, J. Pechousek, C. Gregor, *J. Am. Chem. Soc.* **2007**, *129*, 10929–10936; b) F. Jiao, A. Harrison, J. Jumas, A. V. Chadwick, W. Kockelmann, P. G. Bruce, *J. Am. Chem. Soc.* **2006**, *128*, 5468–5474, and references therein.

[9] a) I. Cesar, A. Kay, J. A. Gonzalez Martinez, M. Grätzel, *J. Am. Chem. Soc.* **2006**, *128*, 4582–4583; b) L. Zhong, J. Hu, H. Liang, A. Cao, W. Song, L. Wan, *Adv. Mater.* **2006**, *18*, 2426–2431.

[10] a) C. Feldmann, *Adv. Mater.* **2001**, *13*, 1301–1303; b) P. Wu, W. Wang, Y. Huang, H. Shen, Y. Lo, T. Tsai, D. Shieh, C. Yeh, *Chem. Eur. J.* **2007**, *13*, 3878–3885.

[11] a) M. Cao, T. Liu, S. Gao, G. Sun, X. Wu, C. Hu, Z. L. Wang, *Angew. Chem.* **2005**, *117*, 4269–4273; *Angew. Chem. Int. Ed.* **2005**, *44*, 4197–4201; b) L. Zhu, H. Xiao, X. Liu, S. Fu, *J. Mater. Chem.* **2006**, *16*, 1794–1797.

[12] a) C. Wu, P. Yin, X. Zhu, C. OuYang, Y. Xie, *J. Phys. Chem. B* **2006**, *110*, 17806–17812; b) B. Tang, G. Wang, L. Zhuo, J. Ge, L. Cui, *Inorg. Chem.* **2006**, *45*, 5196–5200; c) L. Vayssieres, C. Sathe, S. M. Butorin, D. K. Shuh, J. Nordgre, J. Guo, *Adv. Mater.* **2005**, *17*, 2320–2323.

[13] a) C. H. Kim, H. J. Chun, D. S. Kim, S. Y. Kim, J. Park, *Appl. Phys. Lett.* **2006**, *89*, 223103; b) Y. Chueh, M. Lai, J. Liang, L. Chou, Z. L. Wang, *Adv. Funct. Mater.* **2006**, *16*, 2243–2251.

[14] a) C. Jia, L. Sun, Z. Yan, L. You, F. Luo, X. Han, Y. Pang, Z. Zhang, C. Yan, *Angew. Chem.* **2005**, *117*, 4402–4407; *Angew. Chem. Int. Ed.* **2005**, *44*, 4328–4333; b) X. Wen, S. wang, Y. Ding, Z. L. Wang, S. Yang, *J. Phys. Chem. B* **2005**, *109*, 215–220; c) X. Hu, J. C. Yu, J. Gong, Q. Li, G. Li, *Adv. Mater.* **2007**, *19*, 2324–2329.

[15] a) F. Bødker, M. F. Hansen, *Phys. Rev. B* **2000**, *61*, 6826; b) C. H. Kim, H. J. Chun, D. S. Kim, S. Y. Kim, J. Park, J. Y. Moon, G. Lee, J. Yoon, Y. Jo, M. Jung, S. I. Jung, C. J. Lee, *Appl. Phys. Lett.* **2006**, *89*, 223103.

[16] A. Gurlo, R. Riedel, *Angew. Chem.* **2007**, *119*, 3900–3923; *Angew. Chem. Int. Ed.* **2007**, *46*, 3826–3848.

[17] M. Tiemann, *Chem. Eur. J.* **2007**, *13*, 8376–8388.

Received: October 30, 2007
Published online: April 24, 2008

